

Robust Eavesdropping in the Presence of Adversarial Communications for RF Fingerprinting

Andrew Yuan and Rajeev Sahay

Abstract—Deep learning is an effective approach for performing radio frequency (RF) fingerprinting, which aims to identify the transmitter corresponding to received RF signals. However, beyond the intended receiver, malicious eavesdroppers can also intercept signals and attempt to fingerprint transmitters communicating over a wireless channel. Recent studies suggest that transmitters can counter such threats by embedding deep learning-based transferable adversarial attacks in their signals before transmission. In this work, we develop a time-frequency-based eavesdropper architecture that is capable of withstanding such transferable adversarial perturbations and thus able to perform effective RF fingerprinting. We theoretically demonstrate that adversarial perturbations injected by a transmitter are confined to specific time-frequency regions that are insignificant during inference, directly increasing fingerprinting accuracy on perturbed signals intercepted by the eavesdropper. Empirical evaluations on a real-world dataset validate our theoretical findings, showing that deep learning-based RF fingerprinting eavesdroppers can achieve classification performance comparable to the intended receiver, despite efforts made by the transmitter to deceive the eavesdropper. Our framework reveals that relying on transferable adversarial attacks may not be sufficient to prevent eavesdroppers from successfully fingerprinting transmissions in next-generation deep learning-based communications systems.

Index Terms—Adversarial attacks, deep learning, eavesdropping, physical-layer communications, rf fingerprinting

I. INTRODUCTION

AS the number of devices requiring wireless resources has increased, the Internet of Things (IoT) has become the backbone for supporting the vast flux of wireless traffic. The widespread usage of IoT devices has led to the development of security measures to protect wireless networks from adversarial actors. In particular, these measures include, among other protocols, authenticating devices in wireless networks prior to servicing them. For example, cryptographic approaches have been deployed, distributing unique keys at each node to prevent non-authenticated sources from intercepting wireless transmissions. Yet, such software-based security frameworks are susceptible to attacks such as denial of service (DoS) [1], MAC/IP address spoofing [2], and physical tampering [3].

To address the vulnerabilities of software-based security frameworks, hardware-based approaches have recently emerged to perform device authentication. In this capacity, *radio frequency (RF) fingerprinting (RFF)* has attracted attention for its promising ability to identify and authenticate devices

from received signals. Specifically, the inherent imperfections of hardware components are captured in the channel state information (CSI) of received wireless signals and serve as unique identifiers, which can effectively *fingerprint* (i.e., identify) their corresponding transmitter. However, traditional approaches for RFF, such as maximum likelihood estimation (MLE) classifiers [4]–[6] that operate on higher order statistical moments as features, require *a priori* knowledge of the channel and communication protocols, and they often do not have the capacity to generalize to unfamiliar conditions. Alternatively, deep learning has emerged as a promising paradigm for RFF due to its ability to efficiently distinguish RF fingerprints directly from raw in-phase and quadrature (IQ) time samples without requiring the calculation of hand-crafted features in dynamic and congested wireless networks [7], [8].

Standard RFF wireless communications environments consist of a transmitter that broadcasts a wireless signal and a receiver that employs a deep learning model to fingerprint the received signal using its complex baseband representation [9], [10]. In addition, such wireless mediums can also consist of adversaries aiming to compromise the end-to-end RFF process. Although transmitters' fingerprints cannot be mimicked, due to the challenge of replicating the hardware defects of another device, it is common for rogue receivers to eavesdrop on sensitive information. Specifically, due to the broadcast nature of wireless communications, any adversary can effectively sense and locally fingerprint a transmitted signal, reducing the covertness in a communication channel. In a typical over-the-air wiretapping scheme, an eavesdropper may choose to be either active or passive. Active eavesdroppers intercept and modify the message within the transmission, but expose their existence [11]. In contrast, passive eavesdroppers merely receive and decode the intercepted transmission, which may be degraded by environmental factors (e.g., path loss, shadowing, multi-path fading, etc.) [12]. In this work, we focus on the passive scenario and assume that the eavesdropper does not manipulate the transmission but instead attempts to perform device authentication from intercepted signals.

Prior work has shown that transmitters can effectively evade eavesdroppers by injecting adversarial deep learning perturbations into their transmitted signals [13]–[16]. Due to the transferability property of adversarial deep learning attacks [17]–[19], adversarial attacks injected by the transmitter degrade the performance of deep learning-based RFF classifiers at an eavesdropper even when the eavesdropper has imperfect knowledge about the receiver's classification architecture. To mitigate performance degradation from adversarial perturbations at the receiver, the receiver in collaboration with

A. Yuan and R. Sahay are with the Department of Electrical and Computer Engineering, UC San Diego, San Diego, CA, 92093 USA. E-mail: {a1yuan,r2sahay}@ucsd.edu.

This work was supported in part by the UC San Diego Academic Senate under grant RG114404.

the transmitter, filters the adversarial perturbation from the received signal before performing RFF, a method known to be effective in environments where the receiver is aware of the transmitter’s perturbation approach [20], [21].

In this work, we focus on the perspective of the eavesdropper in a deep learning-based RFF framework. Specifically, we develop an approach for an eavesdropper to effectively perform RFF in a wireless environment in which the transmitter and receiver are using adversarial attacks to deceive the eavesdropper. In this capacity, we consider a setup where a transmitting node is broadcasting a message to a receiver, which determines whether the device is trustworthy or untrustworthy by fingerprinting the received signal. Simultaneously, an eavesdropper is intercepting the transmitted signal in an effort to fingerprint the corresponding transmitter for itself. To this end, we develop a time-frequency-based approach, which we theoretically and empirically show to minimize the effect of additive perturbations at the eavesdropper, resulting in RFF performance similar to the receiver at the eavesdropper. Our approach demonstrates that deep learning-based eavesdroppers cannot be evaded through the injection of adversarial attacks thus revealing a major deep learning-based RFF vulnerability, which is particularly concerning in security sensitive applications such as military environments.

Outline and Summary of Contributions: Compared to related work in RFF under adversarial conditions (discussed in Sec. II), we make the following contributions:

- 1) **A robust RFF eavesdropper architecture** (Sec. III-A – III-C): To the best of our knowledge, we are the first to develop a novel methodology for an eavesdropper to perform accurate RFF in the presence of intentional adversarial perturbations injected by the transmitter.
- 2) **Theoretical analysis of eavesdropping framework** (Sec. III-D): We theoretically demonstrate the feasibility of our proposed RFF eavesdropping architecture using temporal-spatial analysis, which effectively eliminates effects of adversarial perturbations that are specifically generated to deceive an eavesdropper.
- 3) **Empirical evaluation on real-world data** (Sec. IV-A – Sec. IV-E): Using a real world RFF dataset, we show that, using our approach, the eavesdropper is able to recover and identify the trustworthiness of devices at a higher performance compared to existing benchmark approaches for adversarial attack mitigation on multiple perturbation designs across a range of potencies in various signal environments.

II. RELATED WORKS

Deep learning, using both convolutional neural network (CNN) and recurrent neural network (RNN) architectures, has been overwhelmingly shown to perform effective RFF on IQ samples [9], [10], [22], [23] as well as on constellation diagrams formed from IQ samples [24]. A common pitfall of deep learning classifiers, however, is their vulnerability to “blindspots” located in high dimensional spaces which drastically sabotage their performances. In domains such as computer vision [25] and speech processing [26], imperceptible adversarial attacks, are crafted to exploit the inherent

vulnerabilities of deep learning models. In device recognition, [27]–[29] have demonstrated the detrimental effects of adversarial attacks in practical scenarios where an attacker crafts a perturbation despite having limited knowledge of the classifier and imperfect CSI. In response, several defenses have been investigated to mitigate the effect of adversarial attacks in RFF. [30]–[32] increased the classifier robustness through various forms of adversarial training, while sacrificing accuracy on clean IQ samples. In addition, other defenses have also been proposed for wireless communications tasks outside of RFF. For example, [33], [34] implemented autoencoders capable of denoising adversarial perturbations injected into modulated signals as a means to fool Automatic Modulated Classification (AMC) models. Our work can be considered orthogonal to such approaches in that we are not interested in developing a defense to improve the robustness of RFF models but rather we show that adversarial attacks crafted specifically to deceive eavesdroppers in a wireless channel can be circumvented.

In AMC tasks, the notion of generating adversarial attacks to fool potential eavesdroppers has been investigated previously. In [13], a transmitter injected adversarial noise into the transmitted symbols in an effort to fool an unwanted eavesdropper while allowing the signal to be recoverable by the legitimate receiver. Similarly, [14] introduced the presence of reconfigurable intelligent surfaces (RISs) in between the transmitter and receiver through manipulating the array of controllable cells that may mitigate channel impairments. Since there may be an eavesdropper, the RIS was adjusted to prevent signal reflection to the eavesdropper while not sacrificing the transmitter and receiver performance. [15] explores privacy-aware communication using a variational autoencoder-based approach that ensures high reconstruction quality for the intended receiver while obscuring sensitive attributes from an eavesdropper, strategically transmitting sensitive information over noisier channels. In contrast to investigating an adversarial scheme to fool the eavesdropper, this is the first work to propose an RFF eavesdropping architecture that can successfully withstand such efforts made by the transmitter.

III. METHODOLOGY

In this section, we model our methodology for performing effective deep learning-based device fingerprinting from an eavesdropper on an intercepted signal containing adversarial perturbations. We begin by defining our signal, channel, and classifier models used for RF fingerprinting by the transmitter, receiver, and eavesdropper (Sec. III-A and III-B). Next, we define the adversarial environment created between the transmitter and receiver to fool an eavesdropper (Sec. III-C). Finally, we develop our method for deep learning-based eavesdroppers to withstand such adversarial environments and show the theoretical performance guarantees of our framework (Sec. III-D). Our overall framework is shown in Fig. 1.

A. Signal and Channel Modeling

As shown in Fig. 1, we consider a wireless communication environment consisting of a transmitter, receiver, and eavesdropper. Both the receiver and the eavesdropper aim to

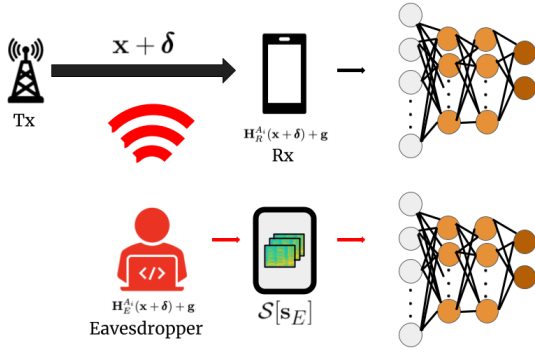


Fig. 1: Our considered system diagram consisting of an RF Fingerprinting architecture in the presence of an eavesdropper.

perform RF fingerprinting on their received signal and classify it as either a trusted or untrusted device. The objective of the transmitter is to transmit a signal that prevents accurate fingerprinting at the eavesdropper while maintaining accurate fingerprinting at the receiver. Simultaneously, the objective of the eavesdropper is to perform accurate fingerprinting on its intercepted signal despite the measures taken by the transmitter to deceive the eavesdropper.

In our framework, we consider a set of $\mathcal{A} = \{A_1, A_2, \dots, A_{|\mathcal{A}|}\}$ transmitters. We further decompose \mathcal{A} into $\mathcal{A} = \mathcal{T} \cup \mathcal{U}$, where \mathcal{T} is the set of trusted transmitters, \mathcal{U} is the set of untrusted transmitters, and $\mathcal{T} \cap \mathcal{U} = \emptyset$. Each transmitter wirelessly transmits $\mathbf{x} = [x[0], \dots, x[\ell - 1]]$ through a channel $\mathbf{h}_R^{A_i} \in \mathbb{C}^\ell$, where $\mathbf{h}_R^{A_i} \in [h_R^{A_i}[0], \dots, h_R^{A_i}[\ell - 1]]$ represents the time-variant RF fingerprint (of A_i), which captures the hardware fingerprints of the transmitter as well as the effects of the wireless channel between the transmitter and receiver. We model the received signal at the receiver by

$$\mathbf{s}_R = \mathbf{H}_R^{A_i} \mathbf{x} + \mathbf{g}, \quad (1)$$

where $\mathbf{H}_R^{A_i} = \text{diag}(\mathbf{h}_R^{A_i}[0], \dots, \mathbf{h}_R^{A_i}[\ell - 1]) \in \mathbb{C}^{\ell \times \ell}$ and $\mathbf{g} \in \mathbb{C}^\ell$ represents complex additive white Gaussian noise (AWGN). In addition, we consider an eavesdropper that will intercept the transmission of \mathbf{x} through $\mathbf{h}_E^{A_i} \in \mathbb{C}^\ell$, where $\mathbf{h}_E^{A_i} \in [h_E^{A_i}[0], \dots, h_E^{A_i}[\ell - 1]]$ also captures the hardware fingerprints of A_i as well as the effects of the wireless channel between the transmitter and the eavesdropper. We assume that the transmitter, receiver, and eavesdropper have knowledge of the channel distribution of $\mathbf{h}_R^{A_i}$, and the eavesdropper also has knowledge of the channel distribution of $\mathbf{h}_E^{A_i}$.

Due to the presence of the eavesdropper, the transmitter attempts to prevent fingerprinting at any unintended receivers by injecting a perturbation $\delta \in \mathbb{C}^\ell$ into \mathbf{x} before transmission. Thus, the true signal transmitted by the transmitter is $\mathbf{x} + \delta$ and the eavesdropper receives

$$\mathbf{s}_E = \mathbf{H}_E^{A_i} (\mathbf{x} + \delta) + \mathbf{g}, \quad (2)$$

where $\mathbf{H}_E^{A_i} = \text{diag}(\mathbf{h}_E^{A_i}[0], \dots, \mathbf{h}_E^{A_i}[\ell - 1]) \in \mathbb{C}^{\ell \times \ell}$. Although unknown at the eavesdropper, the transmitter may use $\delta = \mathbf{0}$ in which case we represent the intercepted signal at the eavesdropper as \mathbf{s}'_E . We further characterize the design of δ

in Sec. III-C. With the injected perturbation, the true signal collected at the receiver is

$$\tilde{\mathbf{s}}_R = \mathbf{H}_R^{A_i} (\mathbf{x} + \delta) + \mathbf{g}, \quad (3)$$

where $\tilde{\mathbf{s}}_R = \mathbf{s}_R$ (from (1)) when the transmitter is not actively perturbing its transmission and, thus, $\delta = \mathbf{0}$.

Since RF fingerprinting at both the receiver and eavesdropper are deep learning-based (as further discussed in Sec. III-B), we map all complex signals to real values $\mathbb{C}^\ell \rightarrow \mathbb{R}^{2\ell}$ using the real and imaginary signal components for compatibility with real-valued neural networks.

B. Receiver Modeling

The objective of the DL model at the receiver is to fingerprint a received signal as belonging to either the set of trusted devices, \mathcal{T} , or the set of untrusted devices \mathcal{U} . Here, the receiver trains a classifier on instances of \mathbf{s}_R , representing the received signal's preamble, which can be used in place of the entire received payload to perform effective device RF fingerprinting without incurring unnecessary training overhead [35], [36].

Formally, we define $\mathcal{X}_{\text{tr}} = \{\mathbf{s}_R^{(i)}, p^{(i)}; i = 1, \dots, N\}$ as the training dataset, where $p^{(i)} \in \{0, 1\}$ denotes if $\mathbf{s}_R^{(i)}$ was transmitted from an untrusted device ($p^{(i)} = 0$) or a trusted device ($p^{(i)} = 1$) and N denotes the number of training samples. Using this dataset, at the receiver, we train a deep neural network (DNN), $\zeta(\cdot, \boldsymbol{\theta}) : \mathbb{R}^{2\ell} \rightarrow \mathbb{R}$, parameterized by $\boldsymbol{\theta}$, to map the i^{th} input sample, $\mathbf{s}_R^{(i)} \in \mathbb{R}^{2\ell}$, (i.e., the preamble of the received signal, which captures the hardware impairments of its transmitter) to the probability $p \in \mathbb{R}$ that the transmitter of the received signal is a trusted device. The DNN takes input (\cdot) , and outputs the the probability that the input was broadcast from a trusted transmitter. Specifically, the trained DNN assigns each testing input $\mathbf{s}_R \in \mathbb{R}^{2\ell}$ a label denoted by $\hat{p}(\mathbf{s}_R, \boldsymbol{\theta}) = \zeta(\mathbf{s}_R, \boldsymbol{\theta})$, where $\zeta(\mathbf{s}_R, \boldsymbol{\theta})$ is the predicted classification probability of \mathbf{s}_R being transmitted from a trusted device. A threshold of 0.5 is used to map $\hat{p}(\mathbf{s}_R, \boldsymbol{\theta})$ to a 0 or 1. During evaluation, we employ the dataset $\mathcal{X}_{\text{te}} = \{\mathbf{s}_R^{(j)}, p^{(j)}; j = 1, \dots, K\}$, where $\mathcal{X}_{\text{tr}} \cap \mathcal{X}_{\text{te}} = \emptyset$ (i.e., no samples overlap in the training and evaluation datasets).

At the receiver, we consider a fully connected neural network (FCNN) architecture. FCNNs consists of L layers, indexed by l , where the l^{th} layer is parameterized by its weights $\boldsymbol{\theta}^{(l)} \in \mathbb{R}^{d_l \times d_{l-1}}$ and biases $\mathbf{b}^{(l)} \in \mathbb{R}^{d_l}$ that are estimated from the training data and d_l and d_{l-1} are hyperparameters denoting the number of units in the l and $l - 1$ layer, respectively. The output of the l^{th} layer is given by $\mathbf{a}^{(l)} = \sigma(\mathbf{z}^{(l)})$, where $\sigma(\cdot)$ is the element-wise activation function, $\mathbf{z}^{(l)} = \boldsymbol{\theta}^{(l)} \mathbf{a}^{(l-1)} + \mathbf{b}^{(l)}$, $\mathbf{a}^{(0)} = \mathbf{s}_R$, and $\mathbf{a}^{(L)} = \hat{p}(\mathbf{s}_R, \boldsymbol{\theta})$. The RFF classifier is trained by minimizing the cross entropy loss function given by

$$\mathcal{L}(\mathbf{s}_R, p, \boldsymbol{\theta}) = -\frac{1}{N} \sum_{i=1}^N p^{(i)} \log(\hat{p}^{(i)}) \quad (4)$$

using stochastic gradient descent (SGD).

C. Evading Eavesdroppers

Due to the broadcast nature of wireless networks, eavesdroppers can intercept and fingerprint transmitted signals using their own surrogate classifier. Despite the eavesdropper and transmitter operating with different classifiers, [37], [38], a perturbation crafted on a particular classifier (e.g., the receiver's classifier) has strong transferability to other classifiers (i.e., the eavesdropper's classifier) trained to perform the same task (e.g., RFF) [39]. Thus, in an effort to evade eavesdroppers, the transmitter, prior to broadcasting \mathbf{x} , injects an adversarial perturbation, $\boldsymbol{\delta}$, which is specifically crafted to fool any potential eavesdroppers and prevent accurate RFF at unauthorized sources while simultaneously ensuring that the receiver is able to recover the signal and perform accurate RFF.

At the transmitter, $\boldsymbol{\delta}$ is crafted, with access to the classifier parameters of the receiver and an approximation of \mathbf{s}_R (obtained by modeling the distributions of $\mathbf{H}_R^{A_i}$ and \mathbf{g} at the transmitters), to find an optimal solution to

$$\min_{\boldsymbol{\delta}} \|\boldsymbol{\delta}\|_p \quad (5a)$$

$$\text{s. t. } \hat{p}(\mathbf{s}_R, \boldsymbol{\theta}) \neq \hat{p}(\tilde{\mathbf{s}}_R, \boldsymbol{\theta}), \quad (5b)$$

$$\zeta(\mathbf{s}_R, \boldsymbol{\theta}) = \zeta(g_{\boldsymbol{\theta}_g}(h_{\boldsymbol{\theta}_h}(\tilde{\mathbf{s}}_R)), \boldsymbol{\theta}), \quad (5c)$$

$$\|\boldsymbol{\delta}\|_2^2 \leq P_T, \quad (5d)$$

$$\tilde{\mathbf{s}}_R \in \mathbb{R}^{2\ell}, \quad (5e)$$

where (5a) denotes the weakest l_p -bounded perturbation, (5b) aims to generate a transferable perturbation, (5c) ensures that the receiver can effectively perform RFF (more specifically described in (12) below), (5d) constrains the power budget P_T , and (5e) ensures that the perturbation remains in the appropriate dimension.

Due to its non-linear nature, a solution to 5 is not guaranteed to exist in which cases a misclassification may never be induced. Moreover, solving (5) is difficult in practice due to its non-linear nature. Therefore, we approximate a solution to (5) using first-order gradient-based adversarial perturbations because they are computationally efficient methods to quickly embed a perturbation in the signal prior to transmission. Unlike gradient-based adversarial perturbations, optimization-based perturbations [40], [41] are computationally expensive, which is undesirable in real-world wireless communication settings where having a fast and simple procedure of injecting a deterrence, while preserving the data rate transmission is crucial. Thus, we consider the fast gradient sign method (FGSM), a *single-step perturbation* [42], and projected gradient descent (PGD), an *iterative perturbation* [43] injected by the transmitter as approximate solutions to (5).

The goal of FGSM is to take a single step, using its total power budget P_T , in the direction that maximizes the classifier's loss function. For an l_2 bounded perturbation, this is given by

$$\boldsymbol{\delta} = \sqrt{P_T} \frac{\nabla_{\mathbf{s}_R} \mathcal{L}(\mathbf{s}_R, p, \boldsymbol{\theta})}{\|\nabla_{\mathbf{s}_R} \mathcal{L}(\mathbf{s}_R, p, \boldsymbol{\theta})\|_2}, \quad (6)$$

and, for an l_∞ -bounded perturbation is given by

$$\boldsymbol{\delta} = \sqrt{P_T} \cdot \text{sign}(\nabla_{\mathbf{s}_R} \mathcal{L}(\mathbf{s}_R, p, \boldsymbol{\theta})), \quad (7)$$

where, in the l_∞ -bounded perturbation, each feature of $\mathbf{s}_R \in \mathbb{R}^{2\ell}$ is perturbed by $\sqrt{P_T}$ in the direction of the sign of the loss function's gradient.

PGD is an iterative extension of FGSM that repeatedly steps in the gradient direction over multiple iterations, using a fraction of its power budget $\beta = 2\sqrt{P_T}/T$ at each iteration, where T is the total number of iterations. Specifically, initializing $\boldsymbol{\delta}^{(0)} = \mathbf{0}$, the l_2 -bounded PGD perturbation on iteration $t + 1$ is given by

$$\boldsymbol{\delta}^{(t+1)} = \text{Proj}_{B_2(0, \sqrt{P_T})} \left(\boldsymbol{\delta}^{(t)} + \beta \frac{\nabla_{\tilde{\mathbf{s}}_R^{(t)}} \mathcal{L}(\tilde{\mathbf{s}}_R^{(t)}, p, \boldsymbol{\theta})}{\|\nabla_{\tilde{\mathbf{s}}_R^{(t)}} \mathcal{L}(\tilde{\mathbf{s}}_R^{(t)}, p, \boldsymbol{\theta})\|_2} \right), \quad (8)$$

where $\boldsymbol{\delta}^{(T)} = \boldsymbol{\delta}$, $\tilde{\mathbf{s}}_R^{(t)} = \mathbf{s}_R + \boldsymbol{\delta}^{(t)}$, and

$$\text{Proj}_{B_2(0, \sqrt{P_T})}(\cdot) = \sqrt{P_T} \frac{\cdot}{\max(\|\cdot\|, \sqrt{P_T})} \quad (9)$$

ensures the perturbation remains inside an l_2 -ball of radius $\sqrt{P_T}$ around \mathbf{s}_R . Similarly, for an l_∞ -bounded PGD attack, the perturbation at iteration $t + 1$, using $\beta = \sqrt{P_T}/T$ and $\boldsymbol{\delta}^{(0)} = \mathbf{0}$, is given by

$$\boldsymbol{\delta}^{(t+1)} = \text{Proj}_{B_\infty(0, \sqrt{P_T})} \left(\boldsymbol{\delta}^{(t)} + \beta \text{sgn}(\nabla_{\tilde{\mathbf{s}}_R^{(t)}} \mathcal{L}(\tilde{\mathbf{s}}_R^{(t)}, p, \boldsymbol{\theta})) \right), \quad (10)$$

where $\boldsymbol{\delta}^{(T)} = \boldsymbol{\delta}$, $\tilde{\mathbf{s}}_R^{(t)} = \mathbf{s}_R + \boldsymbol{\delta}^{(t)}$, and

$$\text{Proj}_{B_\infty(0, \sqrt{P_T})}(\cdot) = \text{clip}(\cdot, \{-\sqrt{P_T}, \sqrt{P_T}\}) \quad (11)$$

ensures the element-wise perturbation remains less than $\sqrt{P_T}$.

The transmitter injects $\boldsymbol{\delta}$ into its signal prior to broadcasting it using either FGSM or PGD. As a result of the transferability of adversarial perturbations, any eavesdropper that intercepts the signal and attempts to perform RFF will classify the signal erroneously. The receiver, on the other hand, is fully aware of the presence of the perturbation in its received signal and is thus able to filter $\boldsymbol{\delta}$ and retain its RFF performance despite the presence of the perturbation.

Due to the effectiveness of Denoising Autoencoders (DAE) in our considered threat model [20], [21] (further discussed in Sec. III-D below), the receiver employs a DAE to reconstruct \mathbf{s}_R from $\tilde{\mathbf{s}}_R$. Specifically, after observing a received transmission, $\tilde{\mathbf{s}}_R \in \mathbb{R}^{2\ell}$, where $P(\tilde{\mathbf{S}}_R | \mathbf{S}_R = \mathbf{s}_R)$ denotes the conditional distribution of a perturbed signal given its clean counterpart, an encoder defined as $h_{\boldsymbol{\theta}_h}(\cdot) : \mathbb{R}^{2\ell} \rightarrow \mathbb{R}^q$ ($q < 2\ell$) is trained to map $\tilde{\mathbf{s}}_R$ into a lower dimensional feature representation. In the reconstruction process, a decoder $g_{\boldsymbol{\theta}_g}(\cdot) : \mathbb{R}^q \rightarrow \mathbb{R}^{2\ell}$ learns to map the lower dimensional feature representation to an approximation of the input without the perturbation. The encoder and decoder are jointly trained to learn the distribution of $P(\mathbf{S}_R | \tilde{\mathbf{S}}_R = \tilde{\mathbf{s}}_R)$ by minimizing the loss of the sample between the perturbed signal $\tilde{\mathbf{s}}_R$ and corresponding unperturbed signal \mathbf{s}_R . Here, we minimize the mean squared error loss, which is given by

$$\mathcal{L}_{\text{MSE}} = \frac{1}{N} \sum_{i=1}^N \frac{1}{2\ell} \sum_{k=1}^{2\ell} (\mathbf{s}_R^{i,k} - g_{\boldsymbol{\theta}_g}(h_{\boldsymbol{\theta}_h}(\tilde{\mathbf{s}}_R^{i,k})))^2. \quad (12)$$

Using SGD, the parameters $\boldsymbol{\theta}_h$ and $\boldsymbol{\theta}_g$ are tuned to reach a local minimum that sufficiently reduces (12). In addition

to $\{\tilde{\mathbf{s}}_R^{(i)}, \mathbf{s}_R^{(i)}; i = 1, \dots, N\}$, we also include $\{\mathbf{s}_R^{(i)}, \tilde{\mathbf{s}}_R^{(i)}; i = 1, \dots, N\}$ as training samples so that the DAE is capable of mapping benign transmissions (i.e., received signals that do not contain adversarial perturbations from the transmitter) to a version of itself.

During deployment, the denoised signal $g_{\theta_g}(h_{\theta_h}(\tilde{\mathbf{s}}_R^{i,j}))$ is forward propagated through the classifier $\zeta(\cdot, \boldsymbol{\theta}) : \mathbb{R}^{2\ell} \rightarrow \mathbb{R}$, yielding $\hat{p}(\mathbf{s}_R, \boldsymbol{\theta}) \in \mathbb{R}$, which denotes the estimated probability with which the received signal was transmitted from a trusted device. As a result of this design, the transmission severely degrades the eavesdropper's ability to gain sensitive information, due to the transferability property of adversarial perturbations, while the receiver can effectively filter the injected noise to obtain an accurate representation of the original transmission, thus allowing for secure communication between the transmitter and receiver.

D. Resilience Analysis of Eavesdropper

Given the design presented in Sec. III-C for communication between a transmitter and receiver, we now shift our focus to the eavesdropper. Here, we develop, and theoretically demonstrate, a stealthy approach for the eavesdropper to perform effective RFF despite the covertness between the transmitter and receiver.

Let us first define the threat model of the eavesdropper. We evaluate the potency of the transmitter's injected perturbation under two distinct environments: (i) Environment A: Partial Receiver Privacy in which the eavesdropper has partial but incomplete knowledge about the classification architecture at the receiver and (ii) Environment B: Complete Receiver Privacy in which the eavesdropper has no knowledge of the classification architecture at the receiver. More specifically, in Environment A, the eavesdropper has knowledge of the receiver's DNN classifier architecture but is blind to its parameters as well as to the DAE whereas, in Environment B, the eavesdropper is blind to both the receiver's DNN architecture and the DAE. We omit from consideration the unrealistic scenario in which the eavesdropper has complete knowledge of the receiver because (i) it is rare (if possible) for an eavesdropper to have perfect knowledge about the signal processing module of the intended receiver in practice [44] and (ii) in such a scenario, the eavesdropper can directly adopt the mitigation strategy at the receiver.

From the eavesdropper's perspective, the goal is to fingerprint \mathbf{s}_E as either a trusted or untrusted device, regardless of any perturbations in the intercepted signal. Existing methods have shown that the transferability of $\boldsymbol{\delta}$ is limited outside of the time domain [45], but such methods lack robustness, since the baseline performance on unperturbed signals outside of the time-domain is typically lower compared to using time domain IQ samples [46]. To address this, we propose to use the short time Fourier transform (STFT) to divide \mathbf{s}_E into equal sized intervals and capture the frequency spectrum of each segment, thus preserving the time-domain information on which DNN-based classifiers are known to be most effective. The STFT of

the received signal at the eavesdropper is defined as

$$S_E^{(n,f)} = \sum_{m=-\infty}^{\infty} s_E[m] w[m-n] e^{-j(2\pi f/M)m}, \quad (13)$$

where $S_E^{(n,f)}$ represents the time-frequency component at time index n and frequency index f , $w[m-n]$ is the Gaussian window function centered at $m = n$, $e^{-j(2\pi f/M)m}$ is the exponential basis function, and M is the total number of discrete Fourier transform bins. Moreover, we use $\mathbf{S}_E = \mathcal{S}[\mathbf{s}_E] \in \mathbb{R}^{T \times F}$ to represent the STFT-based spectrogram of \mathbf{s}_E , where F denotes the number of frequency bins for each segment of \mathbf{s}_E and T is the number of segments of \mathbf{s}_E .

The eavesdropper uses disparate datasets from the receiver, since channel conditions would prevent the eavesdropper from capturing the receiver's exact received signals, denoted by $\mathcal{X}_{\text{tr}}^E = \{\mathbf{S}_E^{(i)}, p^{(i)}; i = 1, \dots, N\}$ and $\mathcal{X}_{\text{te}}^E = \{\mathbf{S}_E^{(j)}, p^{(j)}; j = 1, \dots, K\}$ to train its own DNN, $\xi(\cdot, \mathbf{w}) : \mathbb{R}^{TF} \rightarrow \mathbb{R}$ (where we reshape the spectrogram to maintain compatibility with DNNs), parameterized by \mathbf{w} , to predict the probability, $\hat{p}(\mathbf{S}_E, \mathbf{w}) = \xi(\mathbf{S}_E, \mathbf{w})$, that the transmitter of the received signal is a trusted device. Not only do we show that baseline performance of RFF is maintained on this time-frequency signal representation, in comparison to merely using IQ signals, but we also show that the eavesdropper can perform accurate classification on perturbed RFF signals, owing to feature importance being spread across time and frequency rather than merely being concentrated in the time domain.

We quantify feature importance using SHapley Additive exPlanations (SHAP) [47], which quantifies the contribution of each input feature to the DNN's prediction. Specifically, the SHAP value of $S_E^{(n,f)}$ is defined by

$$\phi_{S_E^{(n,f)}} = \sum_{\mathcal{P} \subseteq \mathcal{Q} \setminus \{S_E^{(i)}\}} \frac{|\mathcal{P}|(|\mathcal{Q}| - |\mathcal{P}| - 1)!}{|\mathcal{Q}|!} (\xi(\mathcal{P} \cup \{S_E^{(n,f)}\}, \boldsymbol{\theta}) - \xi(\mathcal{P}, \boldsymbol{\theta})), \quad (14)$$

where \mathcal{P} is a feature subset of \mathcal{Q} , which contains the set of all features of $\mathcal{S}[\mathbf{s}_E]$, $\zeta(\mathcal{P} \cup \{S_E^{(n,f)}\}, \boldsymbol{\theta}) - \zeta(\mathcal{P}, \boldsymbol{\theta})$ is the difference between the predicted output from the model with and without $S_E^{(n,f)}$, which is summed across all possible feature subsets \mathcal{P} , and $\frac{|\mathcal{P}|(|\mathcal{Q}| - |\mathcal{P}| - 1)!}{|\mathcal{Q}|!}$ is a normalization constant.

Given these definitions, we will now analyze the impact of $\boldsymbol{\delta}$ on \mathbf{S}_E and show that the eavesdropper can effectively perform RFF in its presence. We will employ the following assumptions in our analysis, where each assumption is verified in Sec. IV-C:

Assumption 1: When $\boldsymbol{\psi} = \mathbf{H}_E \boldsymbol{\delta}$ is dispersed across the signal (e.g., when $\boldsymbol{\delta}$ is l_2 bounded), $\mathcal{S}[\boldsymbol{\psi}] \approx 0 \forall f \notin (f_\psi, f_\psi + \Delta_\psi)$ and $f_\psi \gg f_b$, where $f_\psi + \Delta_\psi$ and f_b denotes the bandwidth of $\boldsymbol{\psi}$ and the high-frequency cutoff of \mathbf{S}_E , respectively. Thus, for l_2 -bounded attacks, only the high frequency components of \mathbf{S}_E are impacted.

Assumption 2: When $\boldsymbol{\psi}$ consists of uniformly applied high-magnitude perturbations across the signal (e.g., when $\boldsymbol{\delta}$ is l_∞ bounded), $\mathcal{S}[\boldsymbol{\psi}] \approx 0 \forall f \notin (f_\psi, f_\psi + \Delta_\psi)$ and $f_\psi + \Delta_\psi \ll f_a$, where f_a denotes the low-frequency cutoff of \mathbf{S}_E . Thus,

for l_∞ -bounded attacks only low frequency components of \mathbf{S}_E are impacted.

Assumption 3: When analyzing \mathbf{S}_E , $\phi_{\mathbf{S}_E^{(n, f^*)}} \gg \phi_{\mathbf{S}_E^{(n, \bar{f})}}$, where $f^* \in [f_a, f_b]$, and $\bar{f} \in (-\infty, f_a) \cup (f_b, \infty)$. Thus, high and low frequency components are not pivotal features for prediction in comparison to middle frequency indices.

Given Assumptions 1 – 3, and without loss of generality on the l_p -bound of δ , we present the following theorem to analytically characterize the effect of δ on \mathbf{S}_E .

Theorem 1. *We can model the effect of time-domain induced adversarial perturbations by a transmitter, independent of the l_p – bound and perturbation design, as*

$$|\mathcal{S}[\mathbf{s}_E]| \approx |\mathcal{S}[\mathbf{s}'_E]|, \quad (15)$$

where $|\cdot|$ represents the power spectral density (PSD) of \cdot . Theorem 1 shows that a signal containing $\delta \neq \mathbf{0}$ from the time domain is approximately equal to the same signal in which $\delta = \mathbf{0}$ in the STFT domain, indicating that δ has approximately no impact on the PSD of \mathbf{s}_E .

Proof. See Appendix A. \square

Theorem 1 shows that a transferable perturbation constructed at the transmitter has a negligible effect on the spectrogram of the received signal at the eavesdropper. Therefore, the PSD of the received signal at the eavesdropper, \mathbf{s}_E , when $\delta \neq \mathbf{0}$ is approximately equal to the PSD when $\delta = \mathbf{0}$. Thus, the spectrogram-based RFF classifier at the eavesdropper is expected to retain high classification performance when a signal containing adversarial perturbations is intercepted by the eavesdropper.

IV. PERFORMANCE EVALUATION

In this section, we conduct an empirical evaluation of our proposed eavesdropper-based RFF framework. First, we discuss our empirical setup including our employed dataset, classifier architectures, and experimental parameters (Sec. IV-A). Next, we evaluate the baseline RFF performance of the receiver and eavesdropper (Sec. IV-B) and analyze the feature importance across frequencies to verify Assumptions 1 – 3 (Sec. IV-C). Finally, we evaluate the efficacy of our framework on multiple perturbation designs and potencies and report our results in comparison to several considered baseline approaches (Sec. IV-D and Sec. IV-E).

A. Experimental Setup

We employ a subset of the RF fingerprinting dataset in [48] for our empirical evaluation. Here, we consider a total of $|\mathcal{A}| = 30$ devices, where we select $|\mathcal{T}| = 5$ trusted transmitters and $|\mathcal{U}| = 25$ untrusted transmitters (10 transmitters are unseen and untrusted). In our empirical setup, each transmitter is placed one meter apart in a grid-like fashion, surrounding a single receiver (USRPN210), which records WiFi signals sent over the IEEE 802.11g Channel 11. We assume that the eavesdropper does not have any information about the observations used by the receiver for training, but has obtained its own observations of signals, corresponding to the set of

trusted and untrusted transmitters, which are used for training at the eavesdropper. The receiver and eavesdropper each use 28334 training signals, with 17450 signals received from trusted devices and 10884 signals received from untrusted devices, where no signal between them are the same, and each signal contains $\ell = 256$ samples. We account for dynamically changing conditions by training the eavesdropper and receiver on waveforms collected over four separate days, excluding a distinct day for testing, allowing the models to generalize to varying environments without additional overhead complexity.

In our empirical analysis, we use the perturbation-to-signal ratio (PSR) to quantify the perturbation magnitude. Formally, the PSR is given by

$$\text{PSR [dB]} = \frac{\mathbb{E}[\|\delta\|_2^2]}{\mathbb{E}[\|\mathbf{s}\|_2^2]} \text{ [dB]}, \quad (16)$$

where \mathbb{E} denotes the expected value and \mathbf{s} denotes the corresponding signal including noise, \mathbf{n} , and excluding the adversarial perturbation δ . Here, it is desirable to keep $\text{PSR} < 0$, which can result in a transferable adversarial perturbation, so that the perturbation (i) is not detectable by the eavesdropper, (ii) does not overpower and mask the received signal, and (iii) can be effectively filtered out at the receiver to retain its expected RFF performance.

At the receiver, we train a lightweight RFF FCNN (i.e., a low-parameter classifier for computational efficiency) consisting of 3 hidden layers with 256, 128, and 64 units, respectively, and each hidden layer applies a 50% dropout rate during training. In addition, the DAE architecture that we employ at the receiver consists of 5 hidden layers with 256, 128, 64, 128, and 256 units, respectively, and each hidden layer applies a 50% dropout rate during training. The DAE uses a PSR of -20 dB for training which was empirically determined to maximize both the (i) classification accuracy on instances of $\tilde{\mathbf{s}}_R$ at the receiver and (ii) transferability of the perturbation to the eavesdropper. At the eavesdropper, we model two distinct system knowledge levels (as described in Sec. III-D): Environment A and Environment B. In Environment A, the RFF architecture at the receiver is identical to the receiver’s classifier architecture (excluding the DAE). In Environment B, the eavesdropper’s classifier consists of two hidden layers with 100 and 80 units, respectively. We show that each of the considered lightweight classifiers are able to obtain state-of-the-art RFF accuracy in the absence of adversarial attacks. At the eavesdropper, we use a classifier architecture identical to the receiver except the input layer is 600×1 to accommodate the STFT features. The standard deviation and window length were set to 7 and 50, respectively, after sufficient experimentation. The STFT converts an $\ell = 256$ IQ signal into an $F = 50$ by $T = 12$ spectrogram, corresponding to the 600×1 input layer.

B. RF Fingerprinting Performance

We begin by analyzing the baseline performance of the eavesdropper and receiver on signals in which the transmitter did not inject an adversarial perturbation. Here the eavesdropper and receiver achieve an accuracy of 87.91% and 88.40%, respectively, demonstrating their state-of-the-art RFF classification performance in terms of distinguishing

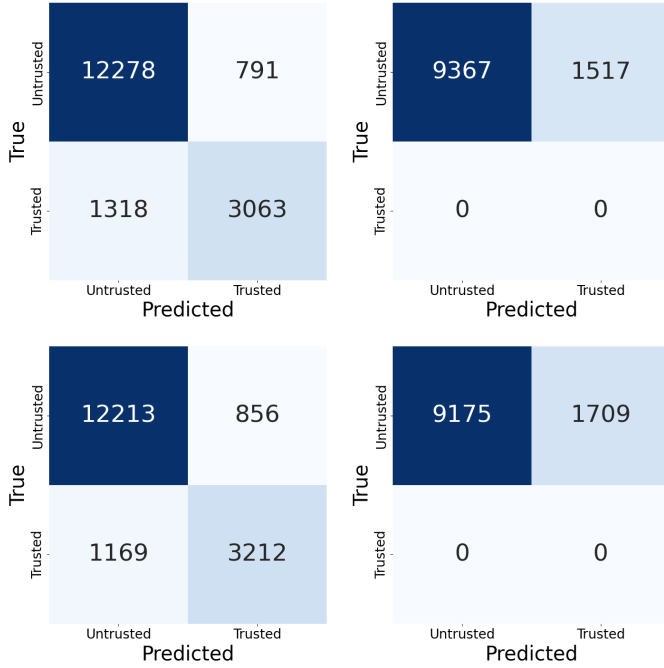


Fig. 2: Confusion matrices showing baseline performance (i.e., with no adversarial attack injected by the transmitter) on signals received from seen and unseen transmitters (top left and top right, respectively) at the eavesdropper and seen and unseen transmitters (bottom left and bottom right, respectively) at the receiver.

trusted and untrusted devices. This accuracy was obtained by evaluating each classifier on *seen* transmitters (i.e., different observations of signals received from transmitters that were in the training set). However, each classifier must be able to effectively identify untrusted transmitters that were *unseen* by the model during training. Thus, in an effort to characterize the performance of the eavesdropper and receiver on *seen* and *unseen* transmitters, we compute the accuracy on a disparate *unseen* testing set. On an *unseen* testing set (containing no signals from trusted devices), the eavesdropper and receiver attain accuracies of 86.06% and 84.30%, respectively, thus showing their ability to identify untrusted devices not present in their training sets. We further show the performance of each setting in Fig. 2, where we see that our proposed eavesdropping framework achieves roughly the same performance as the receiver in authenticating both seen and unseen transmitters.

C. Feature Importance Analysis

We now perform a feature importance analysis of our proposed method to empirically corroborate Theorem 1 and confirm that Assumptions 1 – 3 are valid. Here, we present our results in Environment A as we found that the feature analysis results are nearly identical in Environment B, so we omit them for brevity. Fig 3 shows our feature analysis, assigning SHAP values to the most significant features used by the eavesdropper’s STFT classifier. From Fig. 3, we see that the STFT classifier primarily focuses on mid-range frequencies in adversarial environments indicating that both high frequency and low frequency components have little influence on the classifier’s prediction, thus confirming Assumption 3.

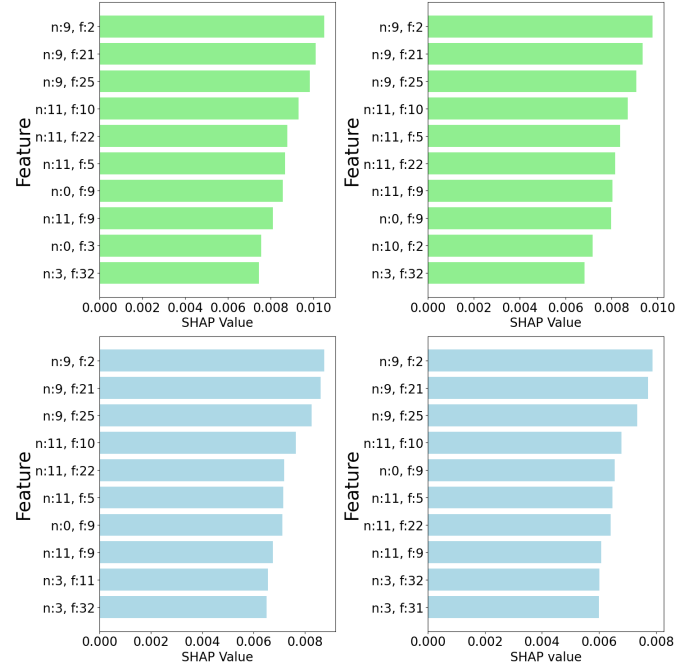


Fig. 3: SHAP values corresponding to l_2 and l_∞ FGSM (top left and top right) and l_2 and l_∞ PGD (bottom left and bottom right) with PSR = -20 dB. The features with the highest importance for RFF are generally middle frequencies, albeit with occasional high and low frequency components present depending on the norm bound.

Moreover, to validate Assumption 1 and Assumption 2, we show the magnitude of the STFT features of the perturbation, δ , in Fig 4 for l_2 and l_∞ -bounded FGSM and PGD perturbations. From Fig. 4, we see that l_2 -bounded perturbations largely impact high frequency components whereas l_∞ -bounded perturbations largely impact low frequency components. Along with Fig. 3, this shows that the features that are the most significantly impacted by adversarial perturbations, independent of the norm bound or perturbation algorithm, are not highly relevant in the classifier’s prediction. This is consistent with Theorem 1 and demonstrates that applying the STFT to adversarially perturbed signals at the eavesdropper has negligible impact on the important features required for effective RFF at the eavesdropper. As a result, adversarial attacks injected by the transmitter are not expected to be highly transferable to the STFT features considered by the eavesdropper, thus allowing the eavesdropper to effectively operate in the presence of adversarial attacks with high performance.

D. Eavesdropper Resilience Against Single-Step Perturbations

Here, we analyze the resilience of our eavesdropper’s RFF approach against single-step FGSM perturbations. Although specific methods do not currently exist to strengthen an eavesdropper’s robustness against adversarial attacks injected by the transmitter, we consider general adversarial mitigation strategies that have been proposed to defend wireless communications classifiers from adversarial attacks as baseline approaches to demonstrate the effectiveness of our proposed method. Specifically, we compare our proposed method to the following baselines: adversarial training [49], Gaussian

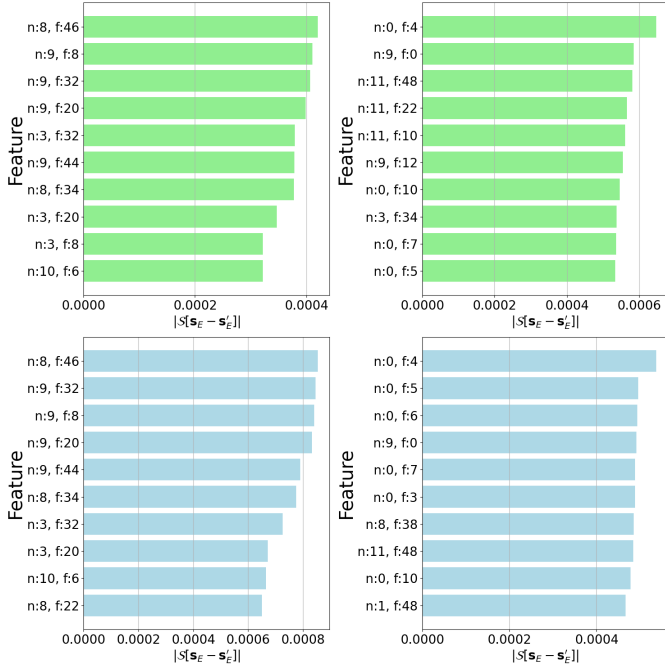


Fig. 4: The top ten features of the spectrogram when the transmitter uses an l_2 - and l_∞ -bounded FGSM perturbation (top left and top right) and l_2 - and l_∞ -bounded PGD perturbation (bottom left and bottom right). Here, l_2 -bounded perturbations generally have a greater impact on high frequency components whereas l_∞ -bounded perturbations generally have a greater impact on low frequency components.

smoothing [50], frequency domain transferability, [51], and amplitude-phase transferability [52]. Adversarial training consists of augmenting the training set with gradient-based adversarial samples between batches of training, where the magnitude of the perturbation is empirically determined such that the classifier results in the highest testing accuracy. Here, we consider two adversarial training baselines: one trained using FGSM perturbations generated according to (6) and (7) and one trained using PGD perturbations generated according to (8) and (10). The Gaussian smoothing approach is trained similarly; instead of gradient-based perturbations, however, samples are added with AWGN, where, the mean and variance of the augmented samples are chosen to maximize the testing accuracy. The frequency-based (FQ) model uses the Discrete Fourier Transform (DFT) of its received signals for training. Similarly, the amplitude-phase (PA) model trains on the amplitude and phase features of each received signal.

In Fig. 5, we show the performance of our approach, in comparison to each considered baseline, in Environment A and Environment B under both l_2 - and l_∞ -bounded perturbations. From Fig. 5, we see that, when the eavesdropper is completely unaware of the perturbation, the transmitter is able to successfully craft a transferable attack to deter the eavesdropper, demonstrated by the eavesdropper’s accuracy dropping to as low as 30%. Our proposed eavesdropper architecture, however, is able to mitigate the effects of the transferable attack, resulting in device identification classification at nearly double the rate (of no resilience) in Environment A and nearly at the same performance as the receiver in Environment B. In

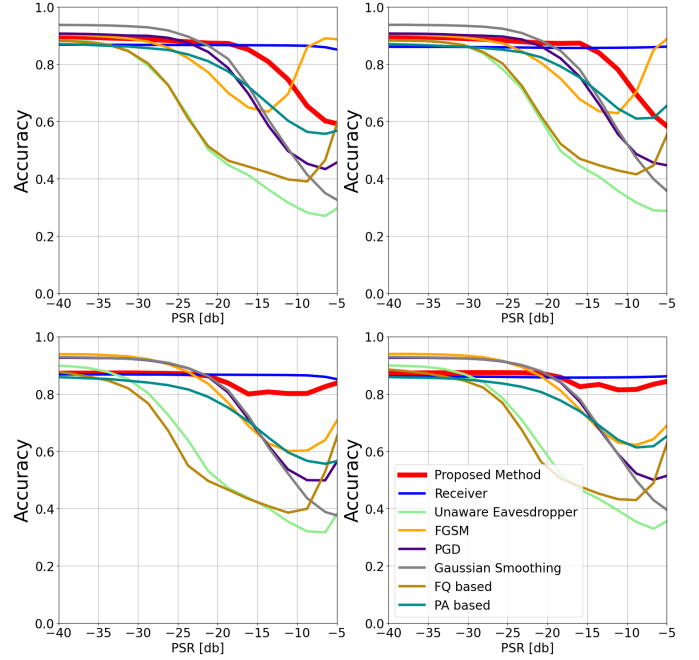


Fig. 5: Eavesdropper’s classification performance against FGSM perturbations injected by the transmitter in comparison to the receiver, unaware eavesdropper, and each considered baseline under l_2 - and l_∞ -bounded perturbations in Environment A (top left and top right), and l_2 - and l_∞ -bounded perturbation in Environment B (bottom left and bottom right). Under our proposed method, the eavesdropper outperforms each considered baseline and approaches the performance of the receiver in certain instances.

contrast, the FGSM and PGD adversarially trained models attain lower RFF classification performance, particularly on high-bounded perturbations, which is the magnitude that the transmitter is likely to use when embedding the perturbation in their transmitted signal as it induces the most potent transferable attack to the eavesdropper (when the eavesdropper is unaware of the perturbation) while delivering state-of-the-art performance at the receiver.

Moreover, in Environment A and B, our proposed method outperforms each considered baseline. For example, in comparison to adversarial training, our proposed method’s performance improves by as high as 40% under the presence FGSM attacks in both environments. While the transmitted perturbations hinder the unaware eavesdropper at PSR < -35 dB and significantly drops in accuracy at -20 dB, our proposed method does not experience impairment until -20 dB, with a rebound after a slight dip at -16 dB, converging towards 80% in Environment B. The robustness of the FGSM and PGD adversarially trained model starts to degrade after PSR = -27 dB), whereas our method remains unaffected throughout nearly the entire PSR range. Under both l_2 and l_∞ attacks in both environments, our proposed STFT-based classifier at the eavesdropper results in greater robustness than applying Gaussian smoothing for PSR ≥ -20 dB. The PA feature representation works well, but has lower overall robustness. Furthermore, when the eavesdropper considers both time and frequency features as in our proposed method, there is a noticeable difference, with respect to the FQ based baseline,

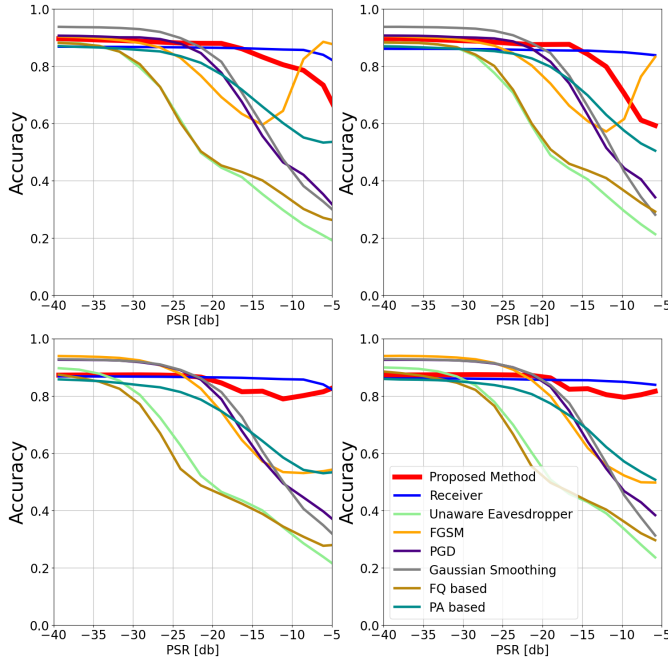


Fig. 6: Eavesdropper’s classification performance against PGD perturbations injected by the transmitter in comparison to the receiver, unaware eavesdropper, and each considered baseline under l_2 - and l_∞ -bounded perturbations in Environment A (top left and top right), and l_2 - and l_∞ -bounded perturbation in Environment B (bottom left and bottom right). Similar to Fig. 5, under our proposed method, the eavesdropper outperforms each considered baseline and again approaches the performance of the receiver in certain instances.

in accuracy of as large as 45% and 40% in Environment A and B, respectively, demonstrating that the use of window filters localizes the adversarial perturbations, preventing them from heavily impairing the eavesdropper’s robustness. Our method outperforms each considered benchmark model under highly potent attacks $\text{PSR} \geq -22$ dB.

As illustrated in Fig. 5, and since solutions to (5), are approximated, (6) and (7) do not always satisfy (5) and induce misclassification. For example, on a single-step attack trained classifier under the presence of FGSM perturbation, instead of proceeding to decline as the magnitude of perturbation rises, the robustness starts to rise. This phenomenon, Catastrophic Overfitting (CO) introduced in [53], suggests that the increased robustness on very strong perturbations is caused by the distortion of the decision boundary. During the adversarial training stage, the classifier may severely overfit to certain examples inducing an over exaggeration in the curvature of the loss function surface [54], [55]. Although the overfitting effect of an FGSM trained eavesdropper achieves higher accuracy than the proposed method and receiver at $\text{PSR} \geq -10$ dB, very high PSRs are unrealistic due to the power budget constraint at the transmitter. In addition, the “turning point” at which overfitting starts to occur is arbitrary, leading to uncertain eavesdropping performance in a desired interval of PSRs.

E. Eavesdropper Resilience Against Iterative Perturbations

We now evaluate our proposed method under PGD adversarial attacks injected by the transmitter. As shown in Fig.

6, when the eavesdropper is unaware of the presence of an attack injected by the transmitter, in both Environment A and Environment B, the accuracy decline begins as early as $\text{PSR} = -33$ dB and steadily decreases to 20%. Our proposed method, on the other hand, in Environment A does not decline in performance until a much stronger perturbation of nearly -19 dB PSR, falling to an accuracy of 60%, providing a maximum improvement in accuracy of 45% at -15 dB. In Environment B, our proposed method is able to withstand the effect of the adversarial attack injected by the transmitter across nearly the entire considered PSR range. In contrast to the unaware eavesdropper’s steady decline in robustness, our implementation endures less dramatic slopes (the unaware eavesdropper experiences a 20% drop in accuracy compared to our method only suffering by 5%) and convergences at 80%.

In Environment A and B, at moderate PSRs (-23 dB), our method maintains an increasing disparity over the FGSM trained eavesdropper in the l_2 and l_∞ cases. A similar phenomenon appears in a multi-step attack trained classifier where the slope of the PGD trained model is steep, experiencing a significant decline in robustness, in contrast to our proposed method. With respect to the performance of the Gaussian smoothed model, although the baseline performance in the absence of an adversarial perturbation is slightly higher than our method, after a moderate PSR (-21 dB), our method achieves greater robustness, which can be observed by the widening gap, where Environment B has a more apparent improvement. In comparison with the existing baselines, our proposed method achieves significantly higher robustness than the FQ based (time-agnostic) model (as high as 45% and 60% in Environment A and B, respectively) and the PA based model (as high as 22% and 31% in Environment A and B, respectively). When considering the receiver’s ability to recover the perturbed transmission, our proposed method allows the eavesdropper to achieve an even greater robustness than the receiver for weak PSRs ($\text{PSR} \leq -20$ dB) in both environments. Comparing Fig. 6 with Fig. 5, the robustness of our proposed method remains consistent against a perturbed transmission regardless of its signal environment and type of perturbation.

V. CONCLUSION

In an effort to mislead eavesdroppers from performing deep learning-based device authentication, while ensuring receivers are not misled, transmitters may inject adversarial perturbations into their broadcast signals. In this work, we developed a robust eavesdropping framework in which the eavesdropper jointly uses time and frequency components to mitigate the effects of such transferable adversarial attacks. We theoretically showed that, on the spatial-temporal features of the perturbed transmission, the effects of the perturbation are localized in regions of the spectrogram that have negligible influence on the classifier. Using a real-world device authentication dataset, we empirically validated our approach and showed its robust performance in comparison to several baseline approaches. Overall, our work reveals that transferable adversarial perturbations are not sufficient for deterring eavesdroppers in deep

learning-based wireless communications. In future work, we will consider the potency of our framework in the adversarial federated learning setting, where additional sources of interference may be present, as well as more robust methods for communications between a transmitter and receiver in the presence of an eavesdropper.

REFERENCES

- [1] Z. Chao-yang, "Dos attack analysis and study of new measures to prevent," in *2011 International Conference on Intelligence Science and Information Engineering*, 2011, pp. 426–429.
- [2] S. Liu, "Mac spoofing attack detection based on physical layer characteristics in wireless networks," in *2019 IEEE International Conference on Computational Electromagnetics (ICCEM)*, 2019, pp. 1–3.
- [3] J. D. Vega Sánchez, L. Urquiza-Aguiar, and M. C. Paredes Paredes, "Physical layer security for 5g wireless networks: A comprehensive survey," in *2019 3rd Cyber Security in Networking Conference (CSNet)*, 2019, pp. 122–129.
- [4] M. W. Lukacs, A. J. Zeqolari, P. J. Collins, and M. A. Temple, "rf-dna" fingerprinting for antenna classification," *IEEE Antennas and Wireless Propagation Letters*, vol. 14, pp. 1455–1458, 2015.
- [5] R. W. Klein, M. A. Temple, and M. J. Mendenhall, "Application of wavelet-based rf fingerprinting to enhance wireless network security," *Journal of Communications and Networks*, vol. 11, no. 6, pp. 544–555, 2009.
- [6] P. Mirowski, D. Milioris, P. Whiting, and T. K. Ho, "Probabilistic radio-frequency fingerprinting and localization on the run," *Bell Labs Technical Journal*, vol. 18, no. 4, pp. 111–133, 2014.
- [7] H. Fu, L. Peng, M. Liu, and A. Hu, "Deep learning-based rf fingerprint identification with channel effects mitigation," *IEEE Open Journal of the Communications Society*, vol. 4, pp. 1668–1681, 2023.
- [8] Y. Bakhti, S. A. Fezza, W. Hamidouche, and O. Déforges, "Ddsa: A defense against adversarial attacks using deep denoising sparse autoencoder," *IEEE Access*, vol. 7, pp. 160 397–160 407, 2019.
- [9] T. Jian, B. C. Rendon, E. Ojuba, N. Soltani, Z. Wang, K. Sankhe, A. Gritsenko, J. Dy, K. Chowdhury, and S. Ioannidis, "Deep learning for rf fingerprinting: A massive experimental study," *IEEE Internet of Things Magazine*, vol. 3, no. 1, pp. 50–57, 2020.
- [10] K. Merchant and B. Nousain, "Enhanced rf fingerprinting for iot devices with recurrent neural networks," in *MILCOM 2019 - 2019 IEEE Military Communications Conference (MILCOM)*, 2019, pp. 590–597.
- [11] H.-N. Dai, H. Wang, H. Xiao, X. Li, and Q. Wang, "On eavesdropping attacks in wireless networks," in *2016 IEEE International Conference on Computational Science and Engineering*, 2016, pp. 138–141.
- [12] A. Chorti, S. M. Perlaza, Z. Han, and H. V. Poor, "Physical layer security in wireless networks with passive and active eavesdroppers," in *2012 IEEE Global Communications Conference*, 2012, pp. 4868–4873.
- [13] M. Z. Hameed, A. György, and D. Gündüz, "The best defense is a good offense: Adversarial attacks to avoid modulation detection," *IEEE Transactions on Information Forensics and Security*, vol. 16, pp. 1074–1087, 2021.
- [14] B. Kim, T. Erpek, Y. E. Sagduyu, and S. Ulukus, "Covert communications via adversarial machine learning and reconfigurable intelligent surfaces," in *2022 IEEE Wireless Communications and Networking Conference (WCNC)*, 2022, pp. 411–416.
- [15] E. Erdemir, P. L. Dragotti, and D. Gündüz, "Privacy-aware communication over a wiretap channel with generative networks," in *ICASSP 2022 - 2022 IEEE International Conference on Acoustics, Speech and Signal Processing (ICASSP)*, 2022, pp. 2989–2993.
- [16] B. He and F. Wang, "Anti-modulation-classification transmitter design against deep learning approaches," *IEEE Transactions on Wireless Communications*, vol. 23, no. 7, pp. 6808–6823, 2024.
- [17] Y. Liu, X. Chen, C. Liu, and D. Song, "Delving into transferable adversarial examples and black-box attacks," in *International Conference on Learning Representations (ICLR)*, 2017.
- [18] F. Tramer, N. Papernot, I. Goodfellow, D. Boneh, and P. McDaniel, "The space of transferable adversarial examples," *arXiv preprint arXiv:1704.03453*, 2017.
- [19] C. Xie, Z. Zhang, Y. Zhou, S. Bai, J. Wang, Z. Ren, and A. L. Yuille, "Improving transferability of adversarial examples with input diversity," in *Proceedings of the IEEE/CVF conference on computer vision and pattern recognition*, 2019, pp. 2730–2739.
- [20] R. Sahay, R. Mahfuz, and A. E. Gamal, "Combating adversarial attacks through denoising and dimensionality reduction: A cascaded autoencoder approach," in *2019 53rd Annual Conference on Information Sciences and Systems (CISS)*, 2019, pp. 1–6.
- [21] R. Sahay, M. Zhang, D. J. Love, and C. G. Brinton, "Defending adversarial attacks on deep learning-based power allocation in massive mimo using denoising autoencoders," *IEEE Transactions on Cognitive Communications and Networking*, vol. 9, no. 4, pp. 913–926, 2023.
- [22] D. Roy, T. Mukherjee, M. Chatterjee, and E. Pasilio, "Rf transmitter fingerprinting exploiting spatio-temporal properties in raw signal data," in *2019 18th IEEE International Conference On Machine Learning And Applications (ICMLA)*, 2019, pp. 89–96.
- [23] W. Wu, S. Hu, D. Lin, and Z. Liu, "Dsln: Securing internet of things through rf fingerprint recognition in low-snr settings," *IEEE Internet of Things Journal*, vol. 9, no. 5, pp. 3838–3849, 2022.
- [24] L. Peng, J. Zhang, M. Liu, and A. Hu, "Deep learning based rf fingerprint identification using differential constellation trace figure," *IEEE Transactions on Vehicular Technology*, vol. 69, no. 1, pp. 1091–1095, 2020.
- [25] N. Akhtar and A. Mian, "Threat of adversarial attacks on deep learning in computer vision: A survey," *IEEE Access*, vol. 6, pp. 14 410–14 430, 2018.
- [26] M. Alzantot, B. Balaji, and M. Srivastava, "Did you hear that? adversarial examples against automatic speech recognition," *arXiv preprint arXiv:1801.00554*, 2018.
- [27] S. Karunaratne, E. Krijestorac, and D. Cabric, "Penetrating rf fingerprinting-based authentication with a generative adversarial attack," in *IEEE International Conference on Communications*, 2021, pp. 1–6.
- [28] B. Liu, H. Zhang, Y. Wan, F. Zhou, Q. Wu, and D. W. K. Ng, "Robust adversarial attacks on deep learning-based rf fingerprint identification," *IEEE Wireless Communications Letters*, vol. 12, no. 6, pp. 1037–1041, 2023.
- [29] D. Roy, T. Mukherjee, and M. Chatterjee, "Machine learning in adversarial rf environments," *IEEE Communications Magazine*, vol. 57, no. 5, pp. 82–87, 2019.
- [30] L. Papangelo, M. Pistilli, S. Sciancalepore, G. Oliveri, G. Piro, and G. Boggia, "Adversarial machine learning for image-based radio frequency fingerprinting: Attacks and defenses," *IEEE Communications Magazine*, vol. 62, no. 11, pp. 108–113, 2024.
- [31] D. Roy, T. Mukherjee, M. Chatterjee, E. Blasch, and E. Pasilio, "Rfal: Adversarial learning for rf transmitter identification and classification," *IEEE Transactions on Cognitive Communications and Networking*, vol. 6, no. 2, pp. 783–801, 2020.
- [32] K. Merchant and B. Nousain, "Securing iot rf fingerprinting systems with generative adversarial networks," in *MILCOM 2019 - 2019 IEEE Military Communications Conference (MILCOM)*, 2019, pp. 584–589.
- [33] M. Z. Hameed, A. György, and D. Gündüz, "The best defense is a good offense: Adversarial attacks to avoid modulation detection," *IEEE Transactions on Information Forensics and Security*, vol. 16, pp. 1074–1087, 2021.
- [34] R. Sahay, D. J. Love, and C. G. Brinton, "Robust automatic modulation classification in the presence of adversarial attacks," in *2021 55th Annual Conference on Information Sciences and Systems (CISS)*, 2021, pp. 1–6.
- [35] S. S. Hanna and D. Cabric, "Deep learning based transmitter identification using power amplifier nonlinearity," in *2019 International Conference on Computing, Networking and Communications (ICNC)*, 2019, pp. 674–680.
- [36] C. Morin, L. S. Cardoso, J. Hoydis, J.-M. Gorce, and T. Vial, "Transmitter classification with supervised deep learning," in *Cognitive Radio-Oriented Wireless Networks: 14th EAI International Conference, CrownCom 2019, Poznan, Poland, June 11–12, 2019, Proceedings 14*. Springer, 2019, pp. 73–86.
- [37] N. Papernot, P. McDaniel, and I. Goodfellow, "Transferability in machine learning: from phenomena to black-box attacks using adversarial samples," *arXiv preprint arXiv:1605.07277*, 2016.
- [38] L. Wu, Z. Zhu, C. Tai *et al.*, "Understanding and enhancing the transferability of adversarial examples," *arXiv preprint arXiv:1802.09707*, 2018.
- [39] Q. Huang, I. Katsman, H. He, Z. Gu, S. Belongie, and S.-N. Lim, "Enhancing adversarial example transferability with an intermediate level attack," in *Proceedings of the IEEE/CVF international conference on computer vision*, 2019, pp. 4733–4742.
- [40] N. Carlini and D. Wagner, "Towards evaluating the robustness of neural networks," in *2017 IEEE Symposium on Security and Privacy (SP)*. Ieee, 2017, pp. 39–57.
- [41] S.-M. Moosavi-Dezfooli, A. Fawzi, and P. Frossard, "Deepfool: a simple and accurate method to fool deep neural networks," in *Proceedings of*

the *IEEE conference on computer vision and pattern recognition*, 2016, pp. 2574–2582.

- [42] I. J. Goodfellow, J. Shlens, and C. Szegedy, “Explaining and harnessing adversarial examples,” *arXiv preprint arXiv:1412.6572*, 2014.
- [43] A. Madry, “Towards deep learning models resistant to adversarial attacks,” *arXiv preprint arXiv:1706.06083*, 2017.
- [44] P. M. Santos, B. R. Manoj, M. Sadeghi, and E. G. Larsson, “Universal adversarial attacks on neural networks for power allocation in a massive mimo system,” *IEEE Wireless Communications Letters*, vol. 11, no. 1, pp. 67–71, 2022.
- [45] R. Sahay, C. G. Brinton, and D. J. Love, “A deep ensemble-based wireless receiver architecture for mitigating adversarial attacks in automatic modulation classification,” *IEEE Transactions on Cognitive Communications and Networking*, vol. 8, no. 1, pp. 71–85, 2022.
- [46] M. Kulin, T. Kazaz, I. Moerman, and E. De Poorter, “End-to-end learning from spectrum data: A deep learning approach for wireless signal identification in spectrum monitoring applications,” *IEEE Access*, vol. 6, pp. 18 484–18 501, 2018.
- [47] S. M. Lundberg and S.-I. Lee, “A unified approach to interpreting model predictions,” *Advances in neural information processing systems*, vol. 30, 2017.
- [48] S. Hanna, S. Karunaratne, and D. Cabric, “Open set wireless transmitter authorization: Deep learning approaches and dataset considerations,” *IEEE Transactions on Cognitive Communications and Networking*, vol. 7, no. 1, pp. 59–72, 2021.
- [49] J. Wang and H. Zhang, “Bilateral adversarial training: Towards fast training of more robust models against adversarial attacks,” in *Proceedings of the IEEE/CVF international conference on computer vision*, 2019, pp. 6629–6638.
- [50] B. Kim, Y. E. Sagduyu, K. Davaslioglu, T. Erpek, and S. Ulukus, “Channel-aware adversarial attacks against deep learning-based wireless signal classifiers,” *IEEE Transactions on Wireless Communications*, vol. 21, no. 6, pp. 3868–3880, 2022.
- [51] Z. Zhang, C. Jung, and X. Liang, “Adversarial defense by suppressing high-frequency components,” *arXiv preprint arXiv:1908.06566*, 2019.
- [52] D. Zhou, N. Wang, H. Yang, X. Gao, and T. Liu, “Phase-aware adversarial defense for improving adversarial robustness,” in *International Conference on Machine Learning*. PMLR, 2023, pp. 42 724–42 741.
- [53] P. Kang and S.-M. Moosavi-Dezfooli, “Understanding catastrophic overfitting in adversarial training,” *arXiv preprint arXiv:2105.02942*, 2021.
- [54] H. Kim, W. Lee, and J. Lee, “Understanding catastrophic overfitting in single-step adversarial training,” in *Proceedings of the AAAI Conference on Artificial Intelligence*, vol. 35, no. 9, 2021, pp. 8119–8127.
- [55] W. He, B. Li, and D. Song, “Decision boundary analysis of adversarial examples,” in *International Conference on Learning Representations*, 2018.

APPENDIX

A. Proof of Theorem 1

Proof. The received signal at the eavesdropper, \mathbf{s}_E , can be rewritten as $\mathbf{s}_E = \mathbf{y} + \boldsymbol{\psi} + \mathbf{g}$, where $\mathbf{y} = \mathbf{H}_E \mathbf{x}$, $\boldsymbol{\psi} = \mathbf{H}_E \boldsymbol{\delta}$, and \mathbf{g} contain the IQ components of the received clean signal, perturbation, and AWGN respectively. The linear nature of the STFT allows us to express the STFT of \mathbf{s}_E as

$$\mathcal{S}[\mathbf{s}_E] = \mathcal{S}[\mathbf{y}] + \mathcal{S}[\boldsymbol{\psi}] + \mathcal{S}[\mathbf{g}]. \quad (17)$$

We can expand $\mathcal{S}[\boldsymbol{\psi}]$ to obtain

$$\mathcal{S}[\boldsymbol{\psi}[n]] = \sum_{\hat{f}=-\infty}^{\infty} \Psi(\hat{f})W(\hat{f}-f)e^{-j2\pi(\hat{f}-f)n} \quad (18)$$

where

$$\Psi(\hat{f}) = \sum_{k=-\infty}^{\infty} \psi[k]e^{-j2\pi\hat{f}k} \quad (19)$$

and

$$W(\hat{f}) = \sum_{k=-\infty}^{\infty} w[k]e^{-j2\pi\hat{f}k} \quad (20)$$

Because $\Psi(\hat{f})$ is ≈ 0 for \hat{f} outside $(f_\psi, f_\psi + \Delta_\psi)$, 18 can be written as

$$\mathcal{S}[\boldsymbol{\psi}[n]] = \sum_{\hat{f}=f_\psi}^{\hat{f}=f_\psi+\Delta_\psi} \Psi(\hat{f})W(\hat{f}-f)e^{-j2\pi(\hat{f}-f)n} \quad (21)$$

Because our window is Gaussian, its spectrum $W(f)$ is also Gaussian. Furthermore, we can bound

$$|\Psi(\hat{f})W(\hat{f}-f)| \leq |\Psi(\hat{f})|Ke^{-\frac{(\hat{f}-f)^2}{2\sigma^2}} \quad (22)$$

where K is a constant. For f in (f_a, f_b) and \hat{f} in $(f_\psi, f_\psi + \Delta_\psi)$, the smallest distance, $|\hat{f}-f|$, is $f_\psi - f_b$. Let κ be a constant where $f_\psi - f_b \geq \kappa\sigma$. Then,

$$e^{-\frac{(\hat{f}-f)^2}{2\sigma^2}} \leq e^{-\frac{(f_\psi-f_b)^2}{2\sigma^2}} \leq e^{-\frac{(\kappa\sigma)^2}{2\sigma^2}} = e^{-\frac{\kappa^2}{2}} \quad (23)$$

Rearranging $f_\psi - f_b \geq \kappa\sigma$ as $f_\psi \geq f_b + \kappa\sigma$ and using Assumption 1 $f_\psi \gg f_b$, κ must be sufficiently large. As $\kappa \rightarrow \infty$, $e^{-\frac{\kappa^2}{2}} \rightarrow 0$. Consequently, 22 and 23 show that $|\Psi(\hat{f})W(\hat{f}-f)| \approx 0$ and therefore, $\Psi(\hat{f})W(\hat{f}-f) \approx 0$, for $f \in (f_a, f_b)$.

The power density spectrum (PSD) of $s_E[n]$ can be expressed as

$$|S_E^{(n,f)}|^2 = |Y^{(n,f)}|^2 + |\Psi^{(n,f)}|^2 + |G^{(n,f)}|^2 + 2\Re[Y^{(n,f)}\Psi^{*(n,f)}] + 2\Re[Y^{(n,f)}G^{*(n,f)}] + 2\Re[\Psi^{*(n,f)}G^{*(n,f)}], \quad (24)$$

where $\Re[\cdot]$ represents the real part of (\cdot) . Knowing that $\Psi(\hat{f})W(\hat{f}-f) \approx 0$, for $f \in (f_a, f_b)$, 18 tells us that $\Psi(n, f) \approx 0$. As a result, the terms containing $\Psi(n, f)$ is ≈ 0 which reduces to

$$|S_E^{(n,f)}|^2 \approx |Y^{(n,f)}|^2 + |G^{(n,f)}|^2 + 2\Re[Y^{(n,f)}G^{*(n,f)}] \quad (25)$$

Recognizing that $|S_E^{(n,f)}|^2 = |Y^{(n,f)}|^2 + |G^{(n,f)}|^2 + 2\Re[Y^{(n,f)}G^{*(n,f)}]$, we can conclude

$$|S_E^{(n,f)}|^2 \approx |S_E^{(n,f)}|^2 \quad (26)$$

for $f \in (f_a, f_b)$.

Similarly, the STFT of an l_∞ perturbation, which is localized in the low frequency range of the spectrum, superimposed with the transmission yields approximately the transmission with $\boldsymbol{\delta} = \mathbf{0}$ in the spatial-temporal representation.

From Assumption 2, $f_\psi + \Delta_\psi \ll f_a$. In 22, for $f \in (f_a, f_b)$ and $\hat{f} \in (f_\psi, f_\psi + \Delta_\psi)$, the smallest value of $|\hat{f}-f|$ is $f_a - (f_\psi + \Delta_\psi)$. Let there be a μ s.t. $f_a - (f_\psi + \Delta_\psi) \geq \mu\sigma$. It follows that

$$e^{-\frac{(\hat{f}-f)^2}{2\sigma^2}} \leq e^{-\frac{(f_a-(f_\psi+\Delta_\psi))^2}{2\sigma^2}} \leq e^{-\frac{(\mu\sigma)^2}{2\sigma^2}} = e^{-\frac{\mu^2}{2}} \quad (27)$$

Analogously, $f_a - (f_\psi + \Delta_\psi) \geq \mu\sigma$ may be rewritten as $f_a \geq (f_\psi + \Delta_\psi) + \mu\sigma$, and since $f_a \gg f_\psi + \Delta_\psi$, μ must be large. Taking the limit as $\mu \rightarrow \infty$, $e^{-\frac{\mu^2}{2}} \rightarrow 0$. Since the upper bound tends to zero for $f \in (f_a, f_b)$, $|\Psi(\hat{f})W(\hat{f}-f)| \rightarrow 0$, and $\mathcal{S}[\boldsymbol{\psi}] \rightarrow 0$, resulting in 24 to simplify as 25 and concluding that $|S_E^{(n,f)}|^2 \approx |S_E^{(n,f)}|^2$ for $f \in (f_a, f_b)$. \square